MICROBIOLOGY

A fitness trade-off between growth and survival governed by Spo0A-mediated proteome allocation constraints in *Bacillus subtilis*

Manlu Zhu, Qian Wang†, Haoyan Mu†, Fei Han, Yanling Wang, Xiongfeng Dai*

Growth and survival are key determinants of bacterial fitness. However, how resource allocation of bacteria could reconcile these two traits to maximize fitness remains poorly understood. Here, we find that the resource allocation strategy of *Bacillus subtilis* does not lead to growth maximization on various carbon sources. Survival-related pathways impose strong proteome constraints on *B. subtilis*. Knockout of a master regulator gene, *spo0A*, triggers a global resource reallocation from survival-related pathways to biosynthesis pathways, further strongly stimulating the growth of *B. subtilis*. However, the fitness of *spo0A*-null strain is severely compromised because of various disadvantageous phenotypes (e.g., abolished sporulation and enhanced cell lysis). In particular, it also exhibits a strong defect in peptide utilization, being unable to efficiently recycle nutrients from the lysed cell debris to maintain long-term viability. Our work uncovers a fitness trade-off between growth and survival that governed by Spo0A-mediated proteome allocation constraints in *B. subtilis*, further shedding light on the fundamental design principle of bacteria.

INTRODUCTION

Rapid growth is a fundamental property of various types of cells including bacterial cells and eukaryotic cells such as yeast cells and tumor cells (*1*–*3*) and is, in principle, advantageous for bacterial fitness (*1*, *3*, *4*). Therefore, growth rate maximization has been proposed to be an important objective of gene regulation in bacterial cells (*1*, *3*, *5*–*7*). In many circumstances, growth rate is used as a convenient parameter to evaluate microbial fitness (*8*–*10*). Recent quantitative studies have suggested that optimal proteome resource allocation enables bacteria to achieve growth rate maximization in various conditions (*1*, *7*, *11*–*16*). Molecularly, global signaling pathways mediated by guanosine tetra- and pentaphosphate [(p)ppGpp] and cyclic adenosine monophosphate (cAMP) enable bacteria to tightly coordinate the biomass growth with proteome resource allocation (*1*, *12*, *15*, *17*).

A fundamental question is whether faster growth simply means higher fitness. Given that the environments in the natural niches of bacteria are often highly fluctuating, bacterial cells must be capable of surviving under stressful conditions such as nutrient deprivation (*18*, *19*). Therefore, surviving capability should constitute another key part of fitness in addition to growth. In this sense, understanding the relationship between growth and survival is of great importance for understanding the fundamental design principles of microbes and is thus a fundamental direction of microbiology. From traditional perspectives, the regulation of growth and survival might, to a large extent, occur at separate life cycle stages and do not necessarily interfere with each other. For example, the *rpoS*-mediated general stress response in *Escherichia coli* is mainly triggered during stationary phase instead of exponential phase (*18*). However, it has recently been found that slow-growing *E. coli* cells (in poor nutrients) could sustain longer during carbon starvation than their fast-growing counterparts (in rich nutrients) due to a decreased maintenance rate (*20*), suggesting that the proteome response during slow growth under nutrient limitation could facilitate the long-term survival of bacterial cells after entry into stationary phase.

It has recently been found that a substantial proteome constraint of inactive ribosomes and other nonflux carrying proteins in *E. coli* might serve other objectives beyond supporting exponential growth, e.g., adaption to nutrient upshift, motility (*1*, *21*–*23*). The implementations of these alternative objectives, which require additional proteome resources, might limit the cellular budget of proteome resources (e.g., ribosomes and metabolic proteins) that are required for supporting biomass growth. Hence, investment on these alternative objectives could occur at the expense of exponential growth, leading to a potential fitness trade-off (improve trait A at the expense of trait B) (*24*). In this sense, the existence of the two key determinants of fitness, growth and survival, raises the important question of whether resource allocation principles of bacteria could simultaneously optimize growth and survival or have to weigh them two against each other.

In this work, we focus on the growth physiology of the model firmicute *Bacillus subtilis*, a master of social behaviors and cell differentiations (*25*–*27*). We find that the strategy of proteome resource allocation in *B. subtilis* leads to balanced investment on growth-trait and survival-trait instead of growth maximization on various carbon sources including the preferred carbon, glucose. Knockout of *spo0A*, encoding a master regulator protein, substantially increases the growth capacity (both rate and yield) that results from the resource reallocation from survival-related pathways to biosynthesis pathways. Nevertheless, such a type of resource reallocation improves growth performance at the expense of survival capability of *B. subtilis*, supporting the existence of a fitness trade-off between growth and survival that governed by Spo0A-mediated proteome allocation constraints in *B. subtilis*.

Hubei Key Laboratory of Genetic Regulation and Integrative Biology, School of Life Sciences, Central China Normal University, Wuhan, Hubei province, China.
*Corresponding author. Email: daixiongfeng@ccnu.edu.cn
†These authors contributed equally to this work.

RESULTS

Spo0A-mediated trade-off between growth and survival in *B. subtilis*

We first characterized the exponential growth rates of *B. subtilis* 168 wild-type strain and its *spo0A*-null derivative strain (*spo0A* encodes the master regulator of sporulation). The growth rates of these two strains were comparable to each other in rich medium (fig. S1). Notably, *spo0A*-null strain had substantially higher growth rates than wild-type strain in minimal media of various carbon sources including glucose, mannose, arabinose and ribose, respectively (Fig. 1A, see typical log-scale exponential growth curves in fig. S2). These results suggest that *B. subtilis* wild-type strain does not pursue growth maximization even on the preferred carbon source, glucose. To explore whether the faster growth of *spo0A*-null strain could confer a fitness advantage, we performed a competitive experiment between *spo0A*-null strain and wild-type strain by coculturing them in the same medium, which is a standard way to compare the relative fitness between two strains (*19*, *28*, *29*). As shown in Fig. 1B, *spo0A*-null strain (green circle) grew much faster than wild-type strain (blue square) when cultured alone in mannose minimal medium. However, during coculture in mannose medium (Fig. 1B, red diamond), it was quickly outcompeted by wild-type strain at early growth stage (150 min to 213 min) and soon completely disappeared during coculture (Fig. 1C). In consistent with this result, the growth of the coculture was arrested at optical density at 600 nm (OD_{600}) ~0.5 at 150 min to 213 min (marked in purple in Fig. 1B) before restoring, suggesting that *spo0A*-null strain had undergone massive cell death during this

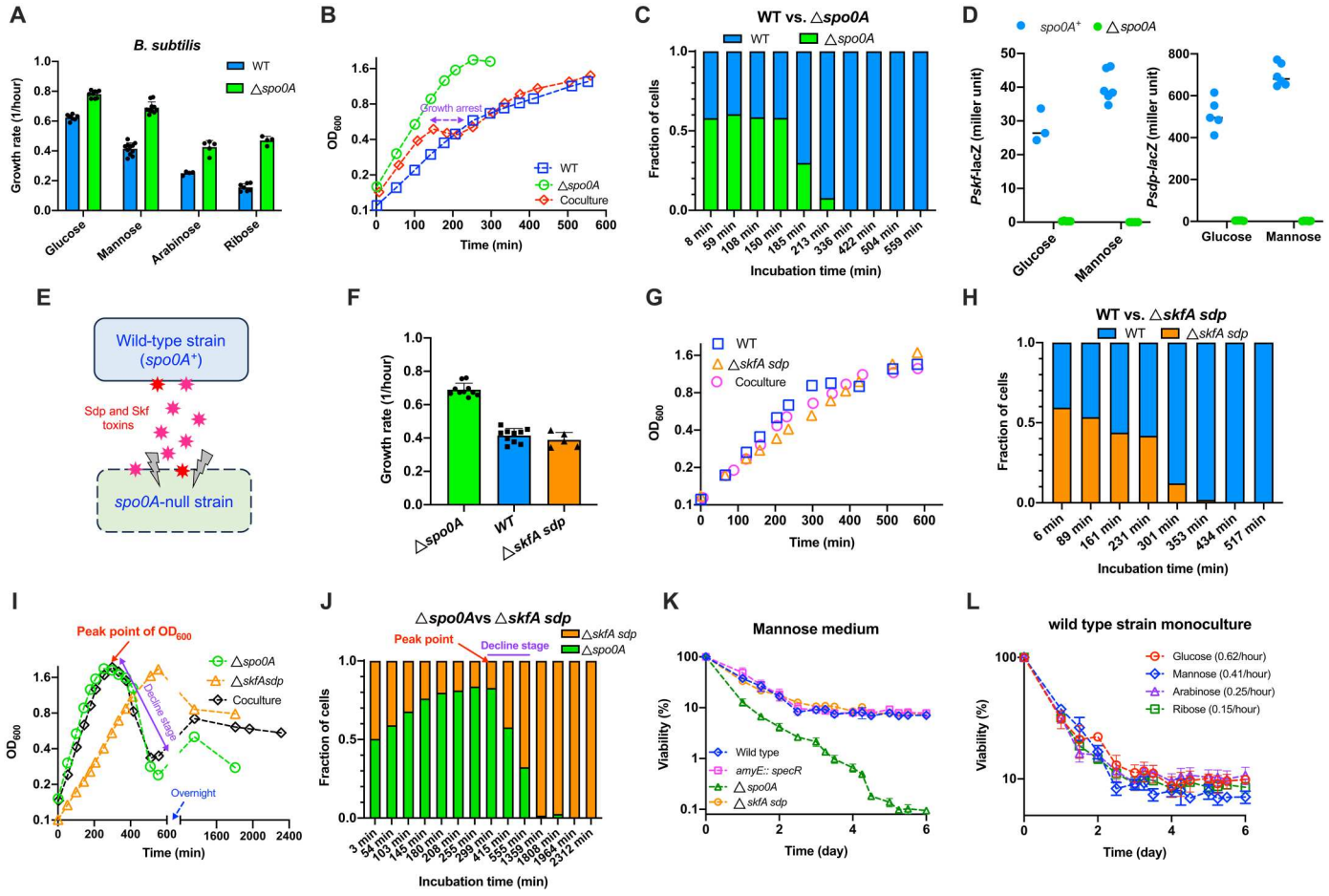

Fig. 1. Spo0A-mediated trade-off between growth and survival in *B. subtilis*. Individual data points and SDs of biological replicates were shown in related panels. (**A**) The exponential growth rates of wild-type (WT) and *spo0A*-null strain. n = 7, 10, 4, and 7 for WT strain and n = 9, 10, 5, and 4 for *spo0A*-null strain growing on glucose, mannose, arabinose, and ribose, respectively. (**B**) The growth curves of WT, *spo0A*-null strain and their coculture in mannose medium. (**C**) The competition experiment of WT versus *spo0A*-null strain during coculturing in mannose medium. The growth curve of coculture corresponds to (B). (**D**) The *lacZ* reporter activities of the two cannibalism operons, *skf* and *sdp*. For P*skf-lacZ* reporter, n = 3 and 6 for *spo0A*$^+$ background and n = 5 and 4 for *spo0A*-null background in glucose and mannose media, respectively. For P*sdp-lacZ* reporter, n = 5 and 6 in glucose and mannose media, respectively, for both *spo0A*$^+$ and *spo0A*-null backgrounds. (**E**) Schematic illustration of the interaction between WT and *spo0A*-null strain. (**F**) The exponential growth rates of WT (n = 10), *spo0A*-null (n = 10), and *skfA sdp*–null strains (n = 5) in mannose medium. (**G**) The growth curves of WT, *skfA sdp*–null strain, and their coculture in mannose medium. (**H**) The competition experiment of WT versus *skfA sdp*–null strain during coculturing in mannose medium. (**I**) The growth curves of *spo0A*-null, *skfA sdp*–null strain, and their coculture in mannose medium. (**J**) The competition experiment of *spo0A*-null versus *skfA sdp*–null strain during coculturing in mannose medium. (**K**) Long-term viability (measured by colony forming units) of four *B. subtilis* strains after nutrient depletion in mannose medium (n = 3). Viability at time zero (when OD_{600} reaches peak point) is set as 100%. (**L**) Long-term viability of WT strain after nutrient depletion on four carbon sources (n = 3). Viability at time zero is set as 100% (n = 3).

short period. Therefore, the faster growth of *spo0A*-null strain failed to confer a fitness advantage. It is known that Spo0A is a key regulator of the cannibalism process that carried out by the *skf* and *sdp* operons in *B. subtilis* (*30*). Cannibalism is a social behavior that occurs during nutrient-limited conditions in which a fraction of cells that begin to enter into sporulation (Spo0A active cells) secrete toxins to kill nonsporulating sibling cells (Spo0A inactive cells) so that the viable cells could feed on the nutrients released by the dead cells to delay the commitment to spore formation (*30*, *31*). β-galactosidase (LacZ) reporter assay showed that the expression of the two cannibalism operons, *skf* and *sdp*, were indeed completely abolished in the *spo0A*-null strain (Fig. 1D). Therefore, *spo0A*-null strain might be directly killed by the cannibalistic toxins secreted by wild-type cells (which are largely immune to toxins as *spo0A*$^+$ background) during coculture (Fig. 1E). We then conducted a competitive experiment between the wild-type strain and the cannibalism-deficient *skfA sdp*–null strain, in which the *skfA* (encoding the spore-killing peptide) as well as the entire *sdpABCDIR* operon were deleted. The *skfA sdp*–null strain had a comparable growth rate to wild-type strain when cultured alone in mannose minimal medium (Fig. 1F); however, it was also quickly outcompeted by wild-type strain during coculture (Fig. 1H; growth curve of the coculture shown in Fig. 1G, pink circles), supporting that cannibalism could be an important factor that cause the fitness defect of *spo0A*-null strain relative to wild-type strain.

We next conducted a competitive experiment between *spo0A*-null and *skfA sdp*–null strains, for which the interference of cannibalism could be eliminated, to see whether the fast-growing *spo0A*-null strain can regain the fitness advantage in this case. The entire coculturing process lasted for more than 36 hours (Fig. 1I, black diamonds). When cultured alone in mannose medium, *spo0A*-null strain again grew much faster than *skfA sdp*–null strain (Fig. 1I, green circles versus orange triangles), and the coculture displayed a similar growth pattern with the monoculture of *spo0A*-null strain (black versus green symbols in Fig. 1I). During the initial ~300 min, *spo0A*-null strain exhibited a fitness advantage over *skfA sdp*–null strain with its population fraction steadily increasing from 50% to more than 80% (Fig. 1J) and OD_{600} of the coculture increased from ~0.15 to the peak point, ~1.95 (black diamonds of Fig. 1I), being consistent with its higher growth capacity and again supporting that fitness defect of *spo0A*-null strain relative to wild-type strain is likely to be related to its devoid of cannibalism.

Notably, the OD_{600} of all the three cultures exhibited a substantial decline immediately after reaching the peak point (Fig. 1I, marked in purple). This phenomenon, resulting from the massive cell lysis of *B. subtilis* population, will be elaborated again later. Although *spo0A*-null strain predominated in the coculture when OD_{600} reached the peak point, its fraction dropped substantially during the abrupt decline stage (marked in purple in Fig. 1, I and J), and furthermore, it was outcompeted by *skfA sdp*–null strain and almost completely disappeared later (Fig. 1J). These results indicate that *spo0A*-null strain might suffer from a long-term survival defect compared with *skfA sdp*–null strain during nutrient deprivation. To test this hypothesis, we investigated the long-term viability of various *B. subtilis* monocultures after nutrient depletion (initiated when OD_{600} reached peak point). When cultured alone in mannose medium, *spo0A*-null strain indeed exhibited a much stronger loss of viability than *skfA sdp*–null strain, wild-type strain, as well as the *amyE::spec*^{R} control strain expressing the spectinomycin-resistance gene (Fig. 1K and table S1), further demonstrating that *spo0A*-null strain indeed suffers a long-term survival defect. Such a survival defect of *spo0A*-null strain here could be partially attributed to its inability of forming spores after nutrient depletion (fig. S3). To further test whether the long-term survival defect of *spo0A*-null strain is related to the *spo0A* gene itself or the indirect effect of its fast growth, we measured the long-term survival of wild-type strain growing on four carbon sources for which the growth rates were varied four times (from 0.15/hour to 0.62/hour). As shown in Fig. 1L, the viability curves of wild-type cells growing on four carbon sources followed similar trends and the cell viability could be maintained constantly at nearly 10% during long-term incubation, supporting that the survival defect of *spo0A*-null strain is related to the *spo0A* gene itself instead of its faster growth than wild-type strain. Overall, the above results demonstrate that *spo0A* knockout stimulated the growth of *B. subtilis* at the expense of long-term survival capability and, hence, led to a fitness trade-off between growth and survival here.

The strategy of proteome resource allocation in *B. subtilis*

Recent quantitative studies have revealed a profound role of proteome resource allocation in controlling bacterial growth (*1*, *2*, *7*, *11*, *14*, *15*). To gain a mechanistic insight into the growth acceleration of *spo0A*-null strain and the growth-survival trade-off described above, we next investigated the proteome resource allocation of *B. subtilis* using quantitative mass spectrometry. Our four-dimensional (4D) label-free mass spectrometry approach captured more than 2500 individual proteins of *B. subtilis* with high reproducibility (tables S2 and S3 and fig. S4). Heatmap and cluster analysis demonstrate a substantial difference in the global gene expression pattern between wild-type and *spo0A*-null strains (Fig. 2A). A first glimpse of the proteome allocation using proteomaps website (https://proteomaps.net) (*32*) shows that *spo0A*-null strain has increased expressions of central biosynthetic pathways including ribosomes and amino acid biosynthetic proteins but a decreased expression of surfactin biosynthesis pathways (*25*, *33*) (belong to the category of cofactor biosynthesis) (Fig. 2B). We further manually quantified the proteome fractions of various specific sectors of social behaviors and cell differentiations, e.g., sporulation, competence, cannibalism, quorum sensing, and antibiotic biosynthesis, which could facilitate the survival and adaption of *B. subtilis* in the harsh natural environments (*25*, *30*, *34*) (table S4). The biosynthetic proteins of surfactin, which participates in regulating cell differentiations and social behaviors (e.g., biofilm, swarming, and quorum sensing) that are crucial for *B. subtilis* to adapt to some stressful environments (*19*, *25*, *35*, *36*), accounted for a larger fraction of the proteome in wild-type strain (~6.25%) than *spo0A*-null strain (~3.85%) (Fig. 2C). Proteins belonging to cannibalism and sporulation groups displayed the most pronounced declining trend in *spo0A*-null background (Fig. 2, D and E), supporting the dominant role of Spo0A in regulating sporulation and cannibalism (*30*). The levels of many other social behavior–related proteins involved in antibiotic production (*34*), competence (*25*), and Rap regulators (regulate competence, sporulation, and surfactin biosynthesis) (*25*) also decreased strongly in *spo0A*-null background (Fig. 2, D to F). Beyond all of this, we also observed a down-regulation in the levels of many specific stress-responsive proteins involved in proteolysis and protein folding, response to toxic substance (Fig. 2, D and G). Collectively, *spo0A* knockout triggers a global down-regulation

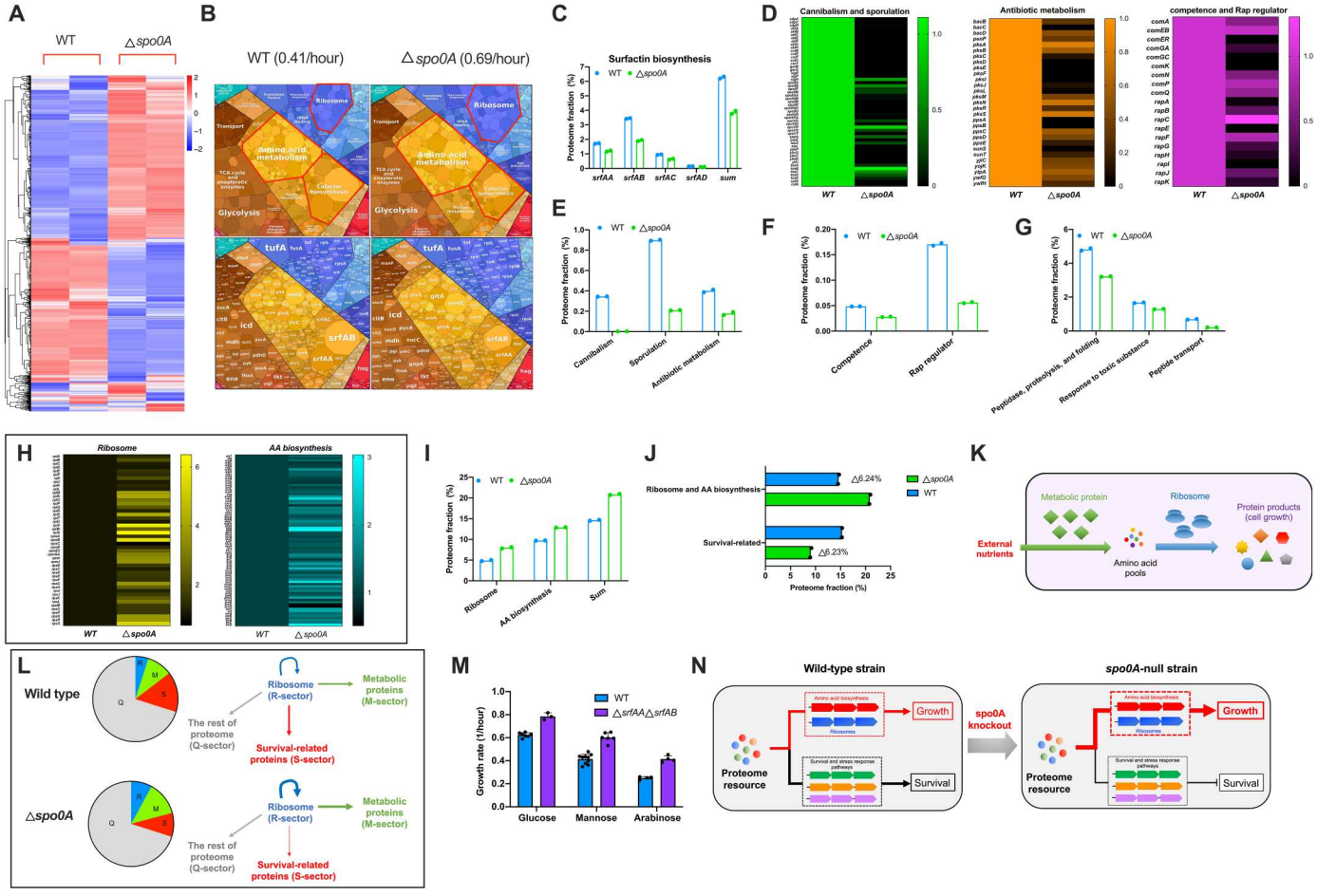

Fig. 2. Proteome resource allocation of *B. subtilis* WT strain and *spo0A*-null strain. The two strains were growing in mannose minimal medium. Data correspond to the average of two biological replicates. (**A**) Heatmap illustration of the proteomes of the two strains. (**B**) Visualization of the proteomic resource allocation of *B. subtilis* by proteomaps website. The subsection term of "mitochondrial biogenesis" inside of the large category "translation" based on Kyoto Encyclopedia of Genes and Genomes (KEGG) categorization (includes both prokaryotes and eukaryotes). The readers should treat these proteins here as translation factors. tRNA, transfer RNA. (**C**) The proteome fractions of surfactin biosynthesis proteins. (**D**) The relative abundances of the typical individual proteins belonging to various social behaviors, cell differentiations, and stress response pathways. (**E** to **G**) The proteome fractions of various survival-related pathways. (**H**) The relative abundances of individual ribosomal proteins and amino acid biosynthesis proteins. (**I**) The proteome fractions of ribosomal proteins and amino acid biosynthesis proteins. (**J**) The changes in the proteome fractions of ribosome and amino acid biosynthesis and survival-related proteins. The survival-related proteins contain all the proteins in (C) and (E) to (G). (**K**) Illustration of the central metabolic pathways. The external nutrients are absorbed and processed by metabolic proteins into amino acid pools, which are further polymerized into proteins by ribosomes to support cell growth. (**L**) The coarse-grained illustration of the proteome resource allocations of WT strain and *spo0A*-null strain. (**M**) Growth rates of WT strain and *srfAA srfAB*–null strain on different carbon sources. Individual data points and SDs of biological replicates were shown (n = 7, 10, and 4 for WT strain growing on glucose, mannose, and arabinose, respectively; n = 3, 6, and 4 for *srfAA srfAB*–null strain growing on glucose, mannose, and arabinose, respectively). (**N**) *spo0A* knockout triggers a global proteome resource reallocation from survival pathways to biosynthesis pathways, boosting growth at the expense of long-term survival.

of various survival-related pathways that are involved in social behavior, cell differentiation, and stress response of *B. subtilis*.

Two major proteome sectors, ribosome and amino acid biosynthesis, exhibited the most pronounced up-regulation of the proteome fraction in *spo0A*-null background, increasing from 4.9 to 8% and from 9.7 to 12.9%, respectively (Fig. 2, H and I, and table S4). Coincidently, the increase in the proteome fraction of ribosome and amino acid biosynthesis (6.2% of the proteome mass) is the same as the decrease in the proteome fraction of survival-related proteins (6.2% of the proteome mass) (Fig. 2J and table S4). To support high protein synthesis rates and rapid growth, both biosynthesis proteins and ribosomes are essential to support high metabolic fluxes with the former one engaging in synthesizing raw materials such as amino acids and the later one being responsible for proteins synthesis (Fig. 2K) (*1*, *2*). The abundance of ribosome, a key determinant of growth rate (*2*, *37*), increased by more than 60% and thus seemed to be sufficient to account for the 60% increase in the growth rate of *spo0A*-null strain relative to the wild-type strain. Moreover, quantitative insight into the proteome allocation strategy of *E. coli* and yeast growing during carbon limitation (*23*) further suggests that the up-regulation of both ribosomes and amino acid biosynthesis (~6.2% of the proteome mass) is sufficient to account for the faster growth of *spo0A*-null strain (0.69/hour) than wild-type strain (0.41/hour) here (fig. S5). On the basis of the recent established phenomenological resource allocation model of bacterial growth, the bacterial proteome can be dissected into three coarse-

grained sectors (*1*, *11*, *12*, *38*–*40*), the metabolic protein sector including enzymes for biosynthesis (M-sector), the ribosome sector (R-sector) and a constant sector (Q-sector) that is not linked to biomass growth (including proteins for metabolic maintenance). The mass fraction of M plus R-sectors is crucial in determining bacterial growth (*1*, *11*, *38*). Overexpression of an unnecessary protein (not useful for biomass growth) imposes a proteome burden and compromises the cellular budget of R-sector and M-sector, further inhibiting bacterial growth (*11*, *40*). In light of our study here, we propose a fourth coarse-grained sector, S-sector, that is, the survival-related pathways. Here, the expression of S-sector imposes a proteome burden and limits the cellular budget of R-sector and M-sector of *B. subtilis*. Knockout of *spo0A* triggers a resource reallocation from S-sector to both R-sector and M-sector (accounting for ~6.2% of the proteome, Fig. 2J) as less ribosomes are required for making S-sector so that more ribosomes are available to increase the levels of R-sector and M-sector (Fig. 2L). The faster growth of *spo0A*-null strain than wild-type strain could thus be quantitatively explained by the proteome resource reallocation model (fig. S5). We next deleted the highly expressed surfactin biosynthesis genes (*srfAA* and *srfAB*) (*25*, *33*) to release the proteome burden of surfactin biosynthesis (~5% of proteome mass, Fig. 2C) and found that the growth of *B. subtilis* was indeed boosted (Fig. 2M), further supporting our resource allocation model here. Collectively, these results support that *spo0A* knockout triggers a global proteome resource reallocation from survival pathways to biosynthesis pathways, boosting bacterial growth at the expense of long-term survival (Fig. 2N).

Cannibalism and cell lysis shape the growth curve of *B. subtilis*

In the growth curves of *spo0A*-null strain (e.g., Fig. 1I), we noted that the OD_{600} exhibited an abrupt decline after growth cessation. Because dry mass/OD_{600} changes very weakly across strains and growth stages (fig. S6), OD_{600} is a reliable reflection of biomass in our condition. Therefore, the abrupt decline of OD_{600} means a substantial decrease of population biomass. The abrupt decline stage also occurred in wild-type strain but at a lower extent than *spo0A*-null strain (figs. S6A and S7, A and B). To gain a more accurate insight into the abrupt decline of population mass, we systematically characterized the growth kinetics of *B. subtilis* using the automatic microplate reader. As shown in Fig. 3 (A to C), the abrupt decline stages (exemplified in Fig. 3B) of growth curves were observed for both *spo0A*-null strain and wild-type strain growing on different carbon sources. Microscopic imaging of bacterial cells at this stage showed large quantities of cell debris, confirming the occurrence of massive cell lysis (Fig. 3D, yellow arrow). During the lysis stage, *spo0A*-null strain and wild-type strain could lose nearly 90 and 60 to 70% of population mass (OD_{600}) in e.g., mannose medium, respectively (Fig. 3B and figs. S6A and S7, A and B). Being consistent with the drop of biomass, cell viability of *B. subtilis* also dropped strongly during this lysis stage (fig. S8). Cell lysis of wild-type strain also occurred strongly in glucose casamino acid (cAA)–rich medium but weakly in LB-rich medium (blue circles in fig. S9, A to D), and moreover, cell lysis was again aggravated in *spo0A*-null strain in both of the two rich media (green triangles in fig. S9, A and B).

In addition to more severe cell lysis compared with wild-type strain, *spo0A*-null strain also displayed a higher growth yield (the peak point of OD_{600}) than wild-type strain on various carbon sources (Fig. 3, A to C, and figs. S3, S6A, and S7, A and B). We wondered whether the difference in growth yield is related to the effect of cannibalism, which could lead to the killing of a fraction of wild-type cells but is completely abolished in *spo0A*-null strain (Figs. 1D and 2E). In support of this assumption, we found that cannibalism-deficient *skfA sdp*–null strain (purple diamonds, Fig. 3, E to G, and fig. S6A) had similar growth yields with *spo0A*-null strain (green triangles, Fig. 3, E to G, and fig. S6A) but higher growth yields than wild-type strain (blue circles, Fig. 3, E to G, and also figs. S6A and S10) on different carbon sources. Moreover, knockout of *spo0A* in the *skfA sdp*–null background did not further increase the growth yields (red triangles, Fig. 3, H to J). These results suggest that cannibalism compromises the growth yield of wild-type strain via killing a fraction of *B. subtilis* cells during late-exponential phase (legend of fig. S10). In support of this notion, in the competitive experiments shown in Fig. 1 (C and H), the killing of the cannibalism-deficient strain (*skfA sdp*–null or *spo0A*-null) by wild-type strain did indeed occur during exponential phase. Hence, a fraction of wild-type cells could also be killed by their counterparts during this stage when cultured alone, further compromising the growth yield.

Cell lysis of *B. subtilis* during nutrient depletion is mediated by autolysins

The massive cell lysis of *B. subtilis* after growth cessation is unusual as this phenomenon were not observed in two fast-growing Gram-negative bacterial species, *E. coli* and *Vibrio natriegens* (fig. S11) (*41*). It is clear that cannibalism is not related to cell lysis here because the cell lysis extent of the cannibalism-deficient *skfA sdp*–null strain was still comparable to that of wild-type strain (fig. S10 and Fig. 3, E to G), not to mention the even more severe lysis that occurred in the cannibalism-deficient *spo0A*-null strain. In addition, the cell lysis extent of *skfA sdp*–null strain also became more severe when its *spo0A* gene was deleted (Fig. 3, H to J), suggesting that the enhanced cell lysis caused by *spo0A* knockout originates from other mechanisms. Given that a robust cell wall is crucial for maintenance of the cell structural integrity, we hypothesized that the cell lysis was mediated by some cell wall autolytic enzymes. We then sought to explore the roles of various autolysins including two major ones, LytC and LytD (*42*, *43*), and two minor ones, LytE and LytF (*44*, *45*) which are involved in cell wall degradation during vegetative growth of *B. subtilis*. As shown in Fig. 4A, the levels of all the four autolysins were much higher in *spo0A*-null strain than in wild-type strain. Knockout of these autolysin genes strongly reduced the cell lysis for both *spo0A*$^+$ and *spo0A*-null backgrounds (Fig. 4, B and C, and figs. S6B and S7C; also see fig. S9, D to F, for rich media). The cell lysis rate was substantially alleviated in both *lytCD*-null and *lytCDEF*-null backgrounds (Fig. 4, D and E). Moreover, when the *lytCDEF* genes had been removed, the residual cell lysis of *spo0A*$^+$ and *spo0A*-null strains became comparable to each other (Fig. 4F), suggesting that the more severe cell lysis of *spo0A*-null strain could attribute to its higher levels of autolysins than wild-type strain.

Peptide uptake is crucial for *B. subtilis* to feed on the lysed cell debris

The cell lysis process observed here was so substantial that we expected the surviving cells could feed on the nutrients released

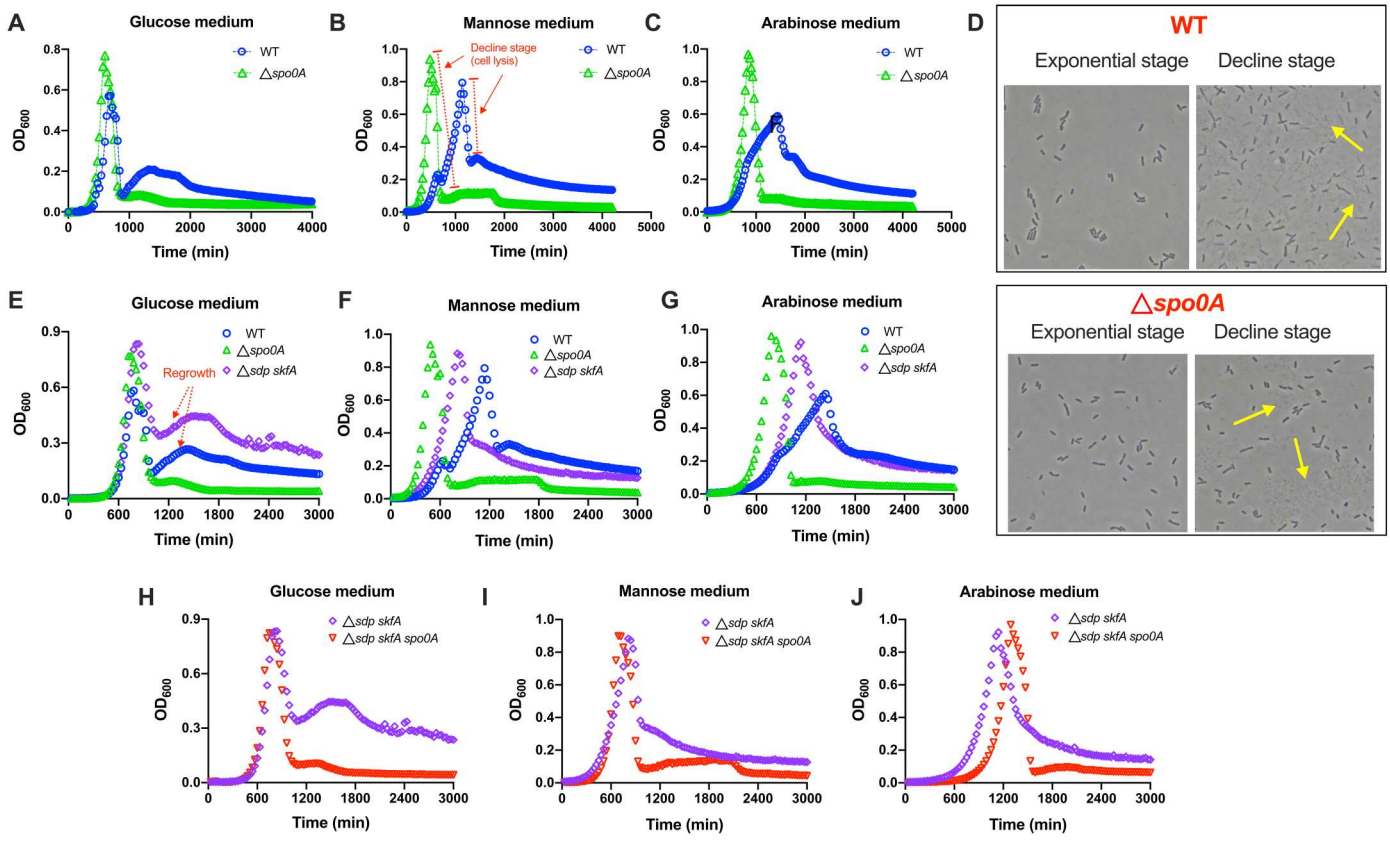

Fig. 3. Cannibalism and cell lysis shape the growth curves of *B. subtilis*. (**A** to **C**) Growth curves of WT and *spo0A*-null strains in glucose, mannose and arabinose minimal media monitored automatically by a microplate reader. The decline stage (cell lysis) is marked in red in (B). Note that the OD_{600} values obtained from a spectrophotometer (figs. S6A and S7, A and B) and the microplate reader here have systematic deviations from each other (for the same cell sample, the OD_{600} value of microplate reader is lower than that obtained by spectrophotometer), but the general trends of growth curves are quite consistent with each other. (**D**) Cell images of WT strain and *spo0A*-null strain during exponential growth stage and decline (cell lysis) stage. The yellow arrow points to some lysed cell debris. (**E** to **G**) The growth curves of WT, *spo0A*-null, and *skfA sdp*–null strains in glucose, mannose, and arabinose media monitored automatically by a microplate reader. (**H** to **J**) The growth curves of *skfA sdp*–null and *skfA sdp spo0A*-null strains in glucose, mannose, and arabinose media monitored automatically by a microplate reader.

from the lysed cells. We noted that the mass of bacterial population in some growth curves underwent a notable second-time increment (regrowth) stage after the abrupt lysis stage (e.g., red arrow, Fig. 3E). Recent studies on *E. coli* have shown that the capability of recycling nutrients released from the dead cells is important for the maintenance of long-term viability of bacterial population (*20*, *46*). We next went back to the competitive experiment between *spo0A*-null strain and *skfA sdp*–null strain (Fig. 1, I and J). We noted an interesting phenomenon here: During the lysis stage of the coculture, the fraction of *spo0A*-null strain dropped quickly from 82% (299 min, peak point of Fig. 1J) to 32% (555 min, Fig. 1J), suggesting that most *spo0A*-null cells had undergone cell lysis during this stage. Then, after a dozen of hours, the mass (OD_{600}) of the coculture exhibited a regrowth, increasing from 0.35 to 0.72; however, the fraction of *spo0A*-null cells dropped further from 32% to only 1% during this period (replotted in Fig. 5A). This result is counterintuitive as *spo0A*-null strain should have a higher growth capacity than *skfA sdp*–null strain when nutrients (released from cell lysis) become available again. Moreover, when cultured alone in mannose medium, the viability of *spo0A*-null strain could actually be maintained for a dozen of hours after the lysis stage (fig. S12). We wondered whether the puzzle here could be due to that *spo0A*-null strain had defects in competing for the nutrients released from the lysed cells against *skfA sdp*–null strain during coculture. We then collected the supernatant of the *spo0A*-null culture after lysis and filtered it to obtain the lysis medium, which contains all the nutrient released from the lysed *spo0A*-null population (Fig. 5B). Both the overnight yield (Fig. 5C) and the growth rate (Fig. 5D) of *spo0A*-null strain were indeed much lower than that of wild-type and *skfA sdp*–null strains when growing in the lysis medium. Being consistent with this observation, *spo0A*-null strain was continuously outcompeted by *skfA sdp*–null strain during coculturing in the lysis medium, even though it had initially been inoculated at a higher fraction (at ~70%) than *skfA sdp*–null strain (at ~30%) (Fig. 5E).

The lower growth capacity of *spo0A*-null strain than wild-type and *skfA sdp*–null strains in the lysis medium suggests that *spo0A*-null strain might be lack of some proteins that are essential for the utilization of nutrients contained in the lysis medium. Proteomics studies showed that the expression of the peptide transport proteins (*dpp*, *app*, and *opp* operons) (*47*–*49*) decreased strongly in *spo0A*-null strain with the expressions of Dpp and App proteins being almost completely abolished (Fig. 5, F and G). In addition, *spo0A* knockout also caused reduced levels of many peptidases (for peptide degradation) (fig. S13). We next investigated the role

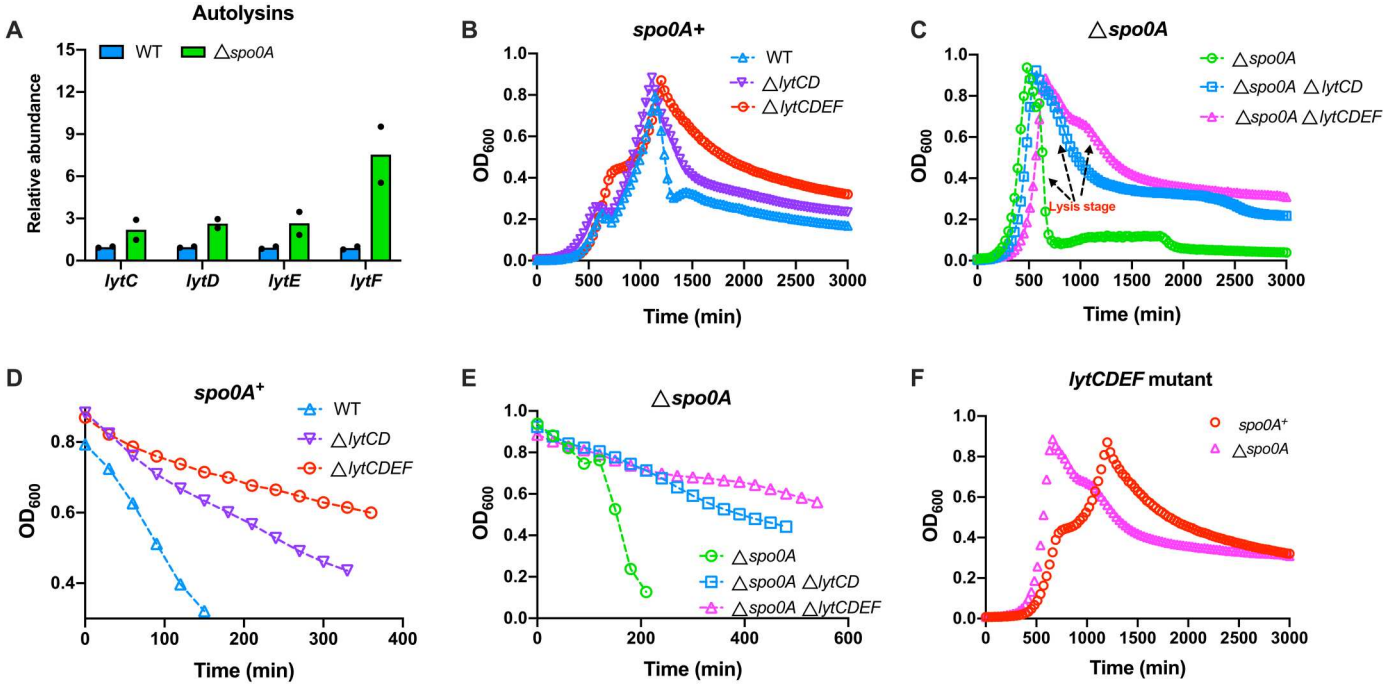

Fig. 4. Cell lysis of *B. subtilis* mediated by autolytic enzymes. (**A**) The relative abundances of autolysins in WT strain and *spo0A*-null strain. Data correspond to the average of two biological replicates. (**B** and **C**) The growth curves of autolysin-deficient strains in *spo0A*$^+$ and *spo0A*-null backgrounds. Growth curves were determined automatically by a microplate reader. (**D** and **E**) The effect of autolysin deficiency on the cell lysis of *B. subtilis spo0A*$^+$ and *spo0A*-null strains. (**F**) The growth curves of *lytCDEF*-null strains in both *spo0A*$^+$ and *spo0A*-null backgrounds. Growth curves were determined automatically by a microplate reader.

of *dpp* and *app* systems in nutrient acquisition from the lysis medium by *B. subtilis*. Notably, the *dpp*-null strain and the *dpp appBC*–null strain exhibited similar growth defects with *spo0A*-null strain in the lysis medium (Fig. 5H), supporting that the peptide uptake indeed acts as an important bottleneck for the utilization of nutrient sources in the lysis medium. Because proteins account for most of bacterial biomass (*50*), the lysis medium is likely to contain many short peptides generated during the process of translation and protein degradation so that peptide transporters and peptidases could enable bacteria to use them. We further found that overexpression of *dpp* and *app* operons could stimulate the growth rate of *spo0A*-null strain in the lysis medium (Fig. 5I), and moreover, Dpp-App overexpression resulted in a notable regrowth of *spo0A*-null strain after the lysis stage in normal glucose and mannose minimal media (orange symbols in Fig. 5, J and K). Collectively, these results demonstrate that after the abrupt lysis stage, *skfA sdp*–null strain (which is *spo0A*$^+$) has a fitness advantage over *spo0A*-null strain during coculture (Fig. 5A) as the former strain harbors more proteins engaged in peptide uptake and metabolism to facilitate the utilization of the nutrients provided by the lysed cell debris. In such scenario, the limitation of peptide utilization imposes a fitness cost on *spo0A*-null strain (Fig. 5L).

DISCUSSION

Growth is crucial for bacterial fitness and recent studies have revealed a profound role of proteome resource allocation in growth control of microbes including bacteria and yeasts (*1*, *7*, *11*–*16*). Meanwhile, increasing evidences show that some other objectives such as adaptation to fluctuating environments (*4*, *51*) and chemotaxis (*52*) are also important. The relation between growth and survival is of special importance as the two traits are key determinants of fitness. However, whether and how resource allocation could reconcile them remains poorly understood. Here, we report a fitness trade-off between growth and survival in *B. subtilis* that is governed by Spo0A-mediated proteome resource reallocation. As an important term in evolutionary biology, the definition of a fitness trade-off is that improving one trait (trait A) at the expense of another trait (trait B) (*24*, *53*–*55*). In our study, there exists a direct competition between growth trait and survival trait for the finite proteome resources. The proteome allocation strategy of wild-type *B. subtilis* strain allows balanced (bet-hedging) investment on growth and survival instead of growth rate maximization on various carbon sources. Such a strategy could allow *B. subtilis* to be better prepared for the upcoming harsh environments after nutrient depletion. Knockout of *spo0A* leads to the proteome resource reallocation from survival and stress response to biosynthesis pathways, thus strongly promoting growth at the expense of long-term survival (Fig. 6). The substantial effect of *spo0A* knockout on stimulating growth of *B. subtilis* is notable given studies on *E. coli* suggest that the growth rates could be nearly maximized in various conditions by global regulatory pathways such as (p)ppGpp and cAMP signaling via optimizing proteome resource allocation (*1*, *5*, *6*, *15*). The proteome burden of survival and stress response is generally believed to be low during exponential stage and thus might not have a notable effect on growth. For example, knockout of *rpoS*, encoding the master regulator of general stress response and stationary phase (*18*), does not have notable effects on the exponential growth rates of *E. coli* under various nutrient conditions (fig. S14) (*20*). The

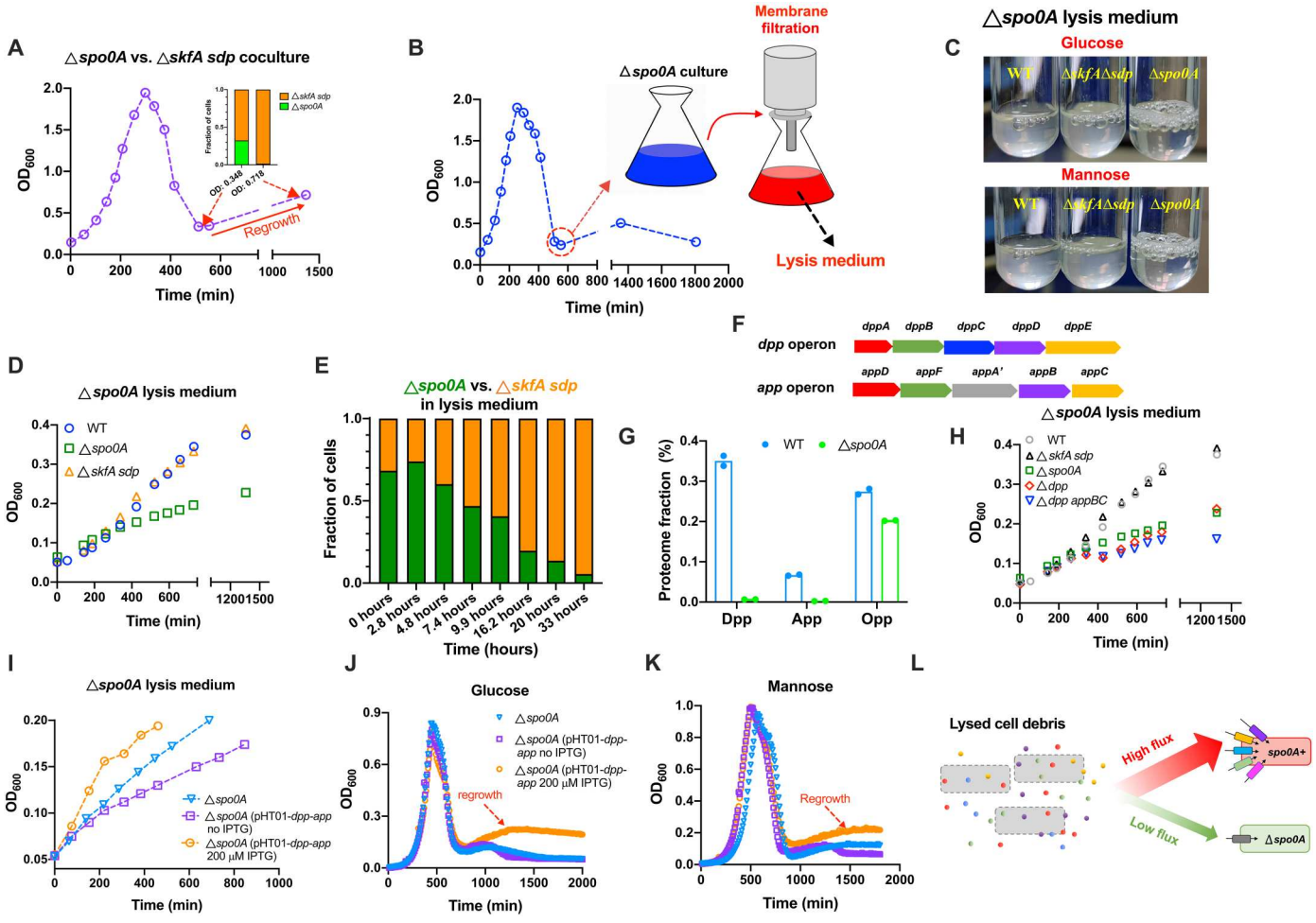

Fig. 5. Peptide transport is crucial for *B. subtilis* to feed on the lysed cell debris. (**A**) The coculture experiment of *spo0A*-null strain and *skfA sdp*–null strain (replotted from Fig. 1, I and J). The relative fractions of these two strains at OD_{600} = 0.348 and 0.718 are shown as subpanels. (**B**) The lysis medium was obtained by filtering the *spo0A*-null cultures at the end of cell lysis stage (the red circle). (**C**) The overnight cultures of WT strain, *spo0A*-null strain, and *skfA sdp*–null strain in the *spo0A* glucose- and mannose-lysis media [means that *spo0A*-null strain had been cultured in glucose or mannose medium before collecting lysis medium as (B)]. (**D**) The growth kinetics of WT strain, *spo0A*-null strain, and *skfA sdp*–null strain in the mannose lysis medium. (**E**) The competition experiment between *spo0A*-null strain and *skfA sdp*–null strain when cocultured in the mannose lysis medium. (**F**) Schematics of the two peptide transporter operons in *B. subtilis*, the *dpp* operon and the *app* operon. (**G**) The proteome fractions of the three peptide transporter systems in WT strain and *spo0A*-null strain. (**H**) The growth kinetics of WT strain, *spo0A*-null strain, *skfA sdp*–null strain, *dpp*-null strain, and *dpp appBC*–null strain in the mannose lysis medium. (**I**) The effect of overexpression of *dpp* and *app* operons on the growth kinetics of *spo0A*-null strain in the mannose lysis medium. The expression of *dpp* and *app* operons was driven by the *grac01* promoter [isopropyl-β-D-thiogalactopyranoside (IPTG)–inducible] of pHT01 vector. (**J** and **K**) The growth curves of *spo0A*-null strain and its *dpp-app*–overexpressing strain in normal glucose and mannose medium determined by a microplate reader. (**L**) Schematics of the coculture of *spo0A*-null strain and *spo0A*$^+$ strain using the lysis medium. The higher levels of peptide transporters and utilization proteins in *spo0A*$^+$ strain confer it a fitness advantage over *spo0A*-null strain.

high proteome investment of *B. subtilis* on survival and stress response during exponential growth might be partially related to the unique life cycle of *B. subtills*, which is often dominated by various types of complex social behaviors during adapting to harsh environments (*25*, *30*, *36*).

Our study shows that Spo0A could act as an important governor of the trade-off relation between growth and survival in *B. subtilis* via shaping the global resource allocation (Fig. 6). Mechanistically, Spo0A might regulate the expressions of downstream target genes in multiple manners. Spo0A is known to be the master regulator of both sporulation and cannibalism processes (*26*, *30*). In the case of sporulation, Spo0A-P (phosphorylated form) is known to directly activate the transcription of various genes including *sigE* and *sigF*, which encode the two major sporulation σ factors (*26*, *56*). In the case of cannibalism, Spo0A-P can directly activate the transcription of *skf* operon and, alternatively, indirectly activate the expressions of both *skf* and *sdp* operons via inhibiting the expression of *abrB*, which encodes the repressor of cannibalism (*30*). For many other target genes that up-regulated by Spo0A, much less are known regarding the underlying regulatory mechanisms. For example, the regulatory effect of Spo0A on surfactin biosynthesis may require the relay of many intermediate regulators such as AbrB, SigH, and PhrC (*35*); The expressions of *dpp* and *app* operons are known to be repressed by CodY via direct binding (*57*). It is possible that there exist some unknown interconnections between Spo0A and CodY regulatory pathways. In

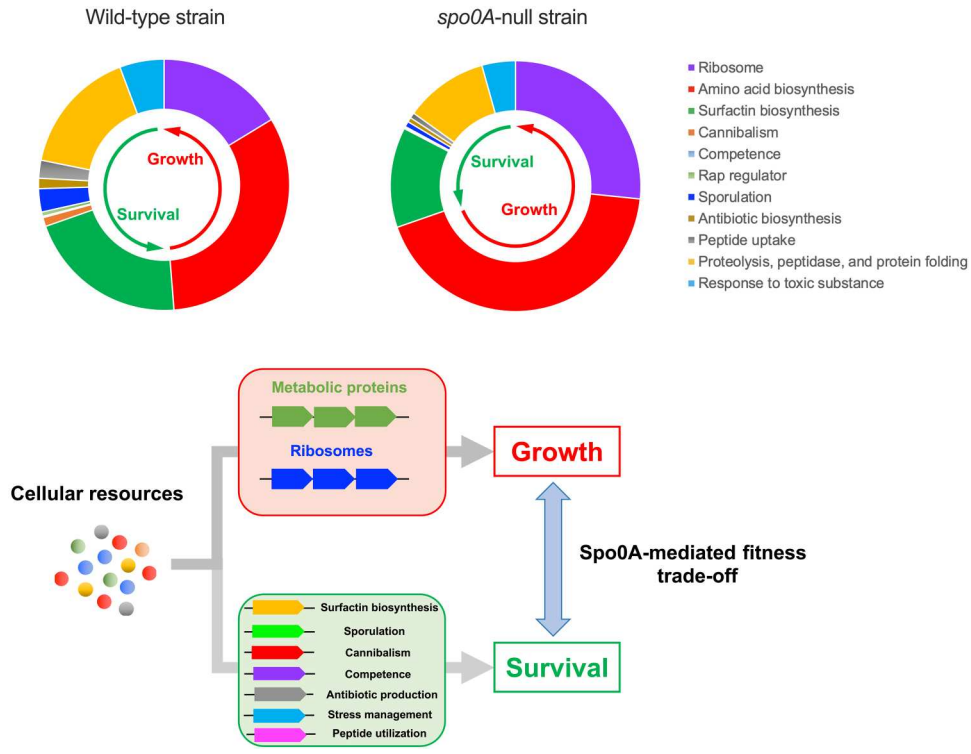

Fig. 6. Spo0A-mediated fitness trade-off between growth and survival that governed by proteome allocation constraints in *B. subtilis*. The cellular resource of bacteria is finite, and *B. subtilis* attempts to balance its proteome investment on biomass growth and survival. In another word, there exists a direct competition between growth trait and survival trait for the finite proteome resources in *B. subtilis*. Spo0A is a key regulator of the trade-off between growth and survival in *B. subtilis*. Compared with WT strain, *spo0A*-null strain has a lower investment on survival-related proteome but a higher investment on growth-related proteome; as a consequence, *spo0A*-null strain has a substantially higher exponential growth rate but a lower long-term fitness than its $spo0A^+$ counterpart (WT strain or *skfA sdp*–null strain). In this sense, Spo0A is an important governor of the fitness trade-off between growth and survival in *B. subtilis*.

addition, the effect of Spo0A on gene expression could also occur in a more general, indirect way via resource allocation. In such scenario, *spo0A* knockout lowers the expressions of survival and stress responsive genes, releasing higher fractions of RNA polymerases and ribosomes for transcribing and translating those ribosome proteins and amino acid biosynthetic proteins. Such an indirect way of gene regulation via resource allocation has previously been shown in the (p)ppGpp signaling pathway of *E. coli* (*15*, *38*).

Our study provides an example of growth-survival trade-off relation that is governed by the Spo0A-mediated proteome constraint in *B. subtilis*. Recent studies of *E. coli* have investigated the effect of the growth status of bacteria on the long-term survival (*20*, *58*). For example, when growth is limited by nutrient quality, proteome response during slow growth could promote the survival of bacteria and slow growth is then accompanied by a higher survival capability (*20*, *58*). However, when growth is limited by other types of stress such as useless protein overexpression or chloramphenicol treatment, slow growth is accompanied with a lower survival capability because the proteome budget related to survival is also likely to be curtailed during such types of growth limitations (*58*). Therefore, the negative relation between growth and survival does not always hold and should depend on the specific proteome response.

Trade-off lies at the core of a cross-kingdom research discipline that seeks to investigate the occurrence of the high degree of biodiversity existing in our ecosystem (*59*, *60*). The trade-off between growth and survival could potentially explain why there exist so many slow-growing bacterial species in nature (e.g., the mycobacterial species) (*61*, *62*). It is known that in the natural environment of bacterial kingdom (e.g., soil), fast-growing species are often not the dominant species (*63*). Moreover, for the same bacterial species, a lot of slow-growing isolates are selected in their natural niches (*64*, *65*). Because bacteria living in their natural niches are often exposed to highly fluctuating environments such as famine-feast cycles (*66*) and a variety of abiotic stresses (*18*), survival instead of growth could be preferentially selected in many cases in which a substantial fraction of cellular resource inside bacteria is allocated to the survival-related proteome to prepare for future uncertainties, thus compromising the growth capacity. Insight into the trade-off mechanism between growth and survival allows us to artificially modulate the fitness landscape of microbes across conditions. Our finding could also have direct implications for the practice of synthetic biology and microbial biotechnology, in which an artificially designed genetic circuit could also have a trade-off relation with the native system of the host bacteria as its operation could take the cellular resources away from supporting cell growth of the host bacteria (*67*, *68*). In this sense, lessons from the trade-off relation between growth and survival in the native bacterial system could be useful in guiding the design of a fitness-robust strain.

Our study has also systematically characterized the growth kinetics of *B. subtilis*. In a classical microbiology textbook, it is generally proposed that bacterial growth follows a four-stages curve: lag phase, exponential phase, stationary phase, and decline phase

(sometimes including a fifth stage called long-term stationary phase) (*69*). When bacteria like *E. coli* enter into stationary phase, the population biomass could stay more or less constant for a certain period (fig. S11). However, the growth of *B. subtilis* does not follow the standard four-stage curve and is strongly affected by cannibalism and cell lysis. During late exponential phase, a fraction of wild-type cells is killed by cannibalism, which compromises the growth yield of wild-type cells. More notably, an abrupt cell lysis stage mediated by autolysins occurs after growth cessation; during this period, 60 to 90% of cells (especially for *spo0A*-null strain) in the population are lysed. Physiologically, such a massive cell lysis of the population could facilitate the long-term fitness of the rest small portion of viable cells by using the nutrients released from lysed cells to sustain for a longer time. Collectively, the cell lysis phenomenon could be regarded as an important survival-related physiological process of *B. subtilis*.

Last, we highlight the physiological role of peptide uptake and metabolism in facilitating bacterial survival under harsh environments such as nutrient starvation. The peptide uptake systems have been widely identified among various bacterial species for a long time (*70*). However, its physiological role in bacteria is less well understood relative to those well-characterized carbon or amino acid transporters (*70*, *71*). Here, we show that for *B. subtilis*, the peptide uptake system is required for recycling the nutrients released from the lysed cells by the rest viable cells, which is crucial for the fitness of *B. subtilis* during nutrient depletion. The lack of peptide uptake systems in *spo0A*-null strain severely compromises its capability of regrowth in the lysis medium. It has recently been shown that the recycling of nutrients released from the dead cells is crucial for the long-term survival of *E. coli* population during stationary phase (*20*, *46*). Given that peptide uptake systems are widely distributed in bacteria, it could be a general mechanism for bacterial cells to recycle nutrients from cell carcasses to maintain viability during stationary phase (nutrient deprivation).

MATERIALS AND METHODS

Strain construction

Strains in the studies were all derivatives *of B. subtilis* 168 (*trpC2*) (*72*). The gene knockout process of *B. subtilis* was based on homologous recombination with the assistance of pDG1730–Sal I (Spc^R) integration vector [with an additional Sal I site at the downstream region of *amyE*′ of pDG1730 (*73*)]. The flanking regions (usually at the range of 600 to 1000 bp) of both downstream and upstream of a specific gene were polymerase chain reaction (PCR) amplified using GoldenStar T6 super PCR mix (Beijing Tsingke Biotech Co., Ltd.) and inserted into the flanking regions of spectinomycin-resistance gene (spc^R) of pDG1730–Sal I (Aat II/Bam HI sites for upstream fragment; Eco RV/Sal I sites for downstream fragment). The resultant vector was linearized by Xho I or Spe I endonuclease digestion and then transformed into the wild-type strain using natural competence. The double-crossover gene knockout transformants were further screened for by colony PCR using 2× GS Taq PCR mix (Genesand Biotech Co., Ltd). The DNA marker (GoldBand DL5,000 DNA Marker) and related electrophoresis reagents such as 50× tris-acetate-EDTA buffer and agarose were purchased from Yeasen Biotech. To construct multiple gene knockout strains, the spc^R of pDG1730 vector was replaced with *catR* (chloramphenicol resistance), *ermR* (erythromycin resistance), *kanR* (kanamycin resistance), and *tetR* (tetracycline resistance), respectively, to obtain gene knockout vectors with different antibiotic markers. Therefore, mutants of multiple gene deletions were constructed sequentially by homologous recombination with different antibiotic resistance markers (e.g., Δ*skfA*::*catR*, Δ*sdpABCDIR*::*ermR* double-knockout strain; Δ*lytC*::*catR*, Δ*lytD*::*ermR*, Δ*lytE*::*kanR*, Δ*lytF*::*tetR* quadruple-knockout strain; *dpp*::*catR*, *appBC*::*kanR* double-knockout strain). The *amyE*::spc^R control strain was constructed by directly transforming the linearized pDG1730–Sal I vector to wild-type strain to screen for the strain with spc^R gene inserted into the *amyE* locus of *B. subtilis*. The concentrations of antibiotics were as below: spectinomycin (Solarbio Life Sciences), 100 μg/ml; chloramphenicol (Coolaber), 5 μg/ml; erythromycin (Solarbio Life Sciences), 2 μg/ml; kanamycin (Coolaber), 7.5 μg/ml; and tetracycline (Coolaber), 15 μg/ml.

To construct the *Psdp-lacZ* and *Pskf-lacZ* reporter strain, the *lacZ* gene of *E. coli* was PCR amplified and inserted into the Bam HI site of the pAX01 integration vector (*74*). The promoter regions of *sdp* operon and *skf* operon were PCR amplified using the *B. subtilis* genome as the template, being further moved into the Xho I/Spe I site of pAX01-*lacZ* vector. The resultant *lacZ* reporter vectors were then transformed and integrated into the genome of *B. subtilis* to obtain the *lacZ* reporter strains.

To construct the peptide transporter overexpression strain, the entire *dpp* operon and *app* operon were PCR amplified (Ultra Hi-Fidelity PCR mix, TianGen) and assembled together into the Bam HI/Sma I site of pHT01 (*75*) using the Gibbon assembly kit, 2X MultiF Seamless Assembly Mix (RK21020) (ABclonal), generating the pHT01-*dpp-app* vector and further transformed into *B. subtilis*.

Medium

B. subtilis was cultured in a modified C-minimal medium (*76*) or LB broth (Coolaber). The basic recipe of C-minimal medium is as follows: K_2HPO_4 (16 g/liter), KH_2PO_4 (4 g/liter), $MnSO_4{\cdot}4H_2O$ (2.32 mg/liter), $MgSO_4{\cdot}7H_2O$ (0.123 g/liter), 12.5 μM $ZnCl_2$, tryptophan (50 mg/liter), and ferric ammonium citrate (22 mg/liter). For all the C-minimal media used, 20 mM NH_4Cl was used as the nitrogen source. Carbon sources used included 0.4% glucose, 0.4% mannose, 0.4% arabinose, and 0.4% ribose. In addition to 0.4% glucose, glucose plus cAA medium also contained 0.4% cAA.

Cell growth measurement

Cell growth was performed either in an air bath shaker (200 rpm, 37°C) or in a 24-well microplate inside a microplate reader. A standard cell culturing procedure contains three steps: seed culture, preculture, and final experimental culture (*12*, *39*, *77*). For the seed culture, cells from a fresh colony were inoculated into LB broth and grew at 37°C to $OD_{600} \approx 1$. The seed culture was then washed and transferred into C-minimal medium supplemented with different carbon sources (the same as the final experimental culture) and grew overnight as precultures. The overnight preculture was inoculated into the same minimal medium at an initial $OD_{600} \approx 0.02$ to 0.03 as the final experimental culture (if the overnight preculture was still within exponential growth stage at OD_{600} from 0.2 to 0.6, then the final culture could be initiated at a higher initial $OD_{600} \approx 0.05$). The growth curve was either manually determined by a Genesys 50 spectrophotometer (Thermo Fisher Scientific) or automatically by an Agilent Biotek Synergy H1 microplate reader. For measuring the exponential growth rate, five to eight OD_{600} points

(generally at the range of 0.05 to 0.7) were measured by a Genesys 50 spectrophotometer to obtain the growth curve, from which the growth rate was calculated on the basis of the exponential range (the linear range at log-scale exponential curve).

Two-strain competitive experiment

Two *B. subtilis* strains were first cultured separately in mannose medium to exponential phase ($OD_{600} \approx 0.6$) and then mixed at a 1:1 ratio (OD_{600}) into the same minimal medium at an initial $OD_{600} \approx 0.1$. At the same time, single strain monoculture was also inoculated at an initial $OD_{600} \approx 0.1$ for comparing the growth curves of monoculture and coculture. The growth curves of the cultures were then determined by a Genesys 50 spectrophotometer (Thermo Fisher Scientific). At different OD_{600} points, the coculture was pipetted into two types of LB solid agars: one with no antibiotics for counting the total cell number and the other one supplemented with specific antibiotics for counting the number of one strain. For example, for the coculture of wild-type strain and *spo0A*-null strain, LB plates with spectinomycin (100 μg/ml) were used to count the cell number of *spo0A*-null strain; for the coculture of wild-type strain and Δ*skfA::catR*, Δ*sdpABCDIR::ermR* double-mutant strain, LB plates with chloramphenicol (5 μg/ml) and erythromycin (2 μg/ml) were applied to count the cell number of Δ*skfA::catR*, Δ*sdpABCDIR::ermR* double-mutant strain.

β-galactosidase assay

The β-galactosidase (LacZ) activities of *Psdp-lacZ* and *Pskf-lacZ* reporter strains were determined by the classical *o*-nitrophenyl β-D-galactopyranoside (ONPG, purchased from GLPBIO) colorimetric method (*12*).

Dry mass measurement

About 100 to 250 ml of cell culture at different growth stages were collected by centrifugation with the supernatant medium being discarded. The cell pellets were then washed by 50 ml of double-distilled H_2O (ddH_2O) and collected again by centrifugation. The OD_{600} of the discarded supernatants was measured to calibrate the loss of cells. The cell pellets were then suspended in 2 ml of ddH_2O and transferred to aluminum pans for baking overnight until reaching a constant weight. The weights of cell pellets were then normalized by the calibrated OD_{600}.

Determination of sporulation efficiency

The sporulation efficiency (spore fraction) of *B. subtilis* was assayed by the heat shock method (*78*). The total viable cell count (N_{total}) of *B. subtilis* was determined by plating the serially diluted samples on LB solid agar media. For counting the spores of *B. subtilis*, the cultures were first subject to 80°C heating for 20 min to kill the vegetative cells and then counted by plating to get the N_{spore} (the number of spores). The sporulation efficiency thus equals to N_{spore}/N_{total}.

Proteomics

The proteomic process generally followed the same procedure as described previously for *E. coli* (*51*) and detailed again below. Exponential culture of *B. subtilis* (30 ml; OD_{600}, 0.6) was collected by centrifugation (4°C, 8500 rpm for 5 min) in a prechilled 50-ml centrifuge tube (Nest Biotech). The cell pellets were then washed twice by phosphate-buffered saline, dried by a speed vacuum concentrator (CV600, Beijing JM Technology Co., Ltd.), and stored at a −80°C freezer before proteomic analysis. The 4D label-free proteomic experiment (*79*) was performed by Jingjie PTM Biolabs (Hang Zhou). For details: The cell pellets were first subject to ultrasonication in lysis buffer [8 M urea, 1% Triton X-100, 10 mM dithiothreitol (DTT), 1% protease inhibitor cocktail, and 2 mM EDTA]. The cell debris was then removed by centrifugation (4°C, 12,000*g* for 10 min) and the supernatant was transferred into a new centrifuge tube for measuring protein concentrations using a The bicinchoninic acid assay (BCA) kit. Protein samples were next pelleted by 20% trichloroacetic acid (TCA) at 4°C for 2 hours and then collected with centrifugation (4500 g/min) for 5 min. The precipitates were washed for twice by precooled acetone and further supplemented with 200 mM triethylammonium bicarbonate (TEAB). Trypsin was then added at 1:50 trypsin-to-protein mass ratio for digestion overnight. The solution was further reduced with 5 mM DTT for 30 min at 56°C and alkylated with 11 mM iodoacetamide for 15 min at room temperature in darkness. Last, the peptides were desalted by a C18 SPE column. Solvent A (0.1% formic acid, 2% acetonitrile) and solvent B (0.1% formic acid, 100% acetonitrile) were then used for the following peptides separation and Ultra Performance Liquid Chromatography (UPLC) procedures. The peptides were dissolved in solvent A and separated by the NanoElute UPLC system. The flow setting of UPLC was as follows: 0 to 43 min, 6 to 22% B; 43 to 55 min, 22 to 30% B; 55 to 58 min, 30 to 80% B; 58 to 61 min, 80% B; flow rate, 450 nl/min. After UPLC separation, the peptide was set into capillary ionization source for ionization and further analyzed by the timsTOF Pro mass spectrometry system. The electrospray voltage applied was set at 1.6 to 1.8 kV. Both the original peptide ion and its secondary fragments were detected and analyzed by high-resolution time of flight (TOF). The mass/charge ratio scan range was 100 to 1700 for full scan. Precursors with charge states 0 to 5 were selected for fragmentation, and 10 PASEF-MS/MS scans were acquired per cycle. The dynamic exclusion was set to 30 s. The mass spectra data were searched against the SwissProt *B. subtilis* 168 databases and analyzed by Maxquant software (*80*), which gave the information of both label-free quantification (LFQ) intensity and intensity based absolute quantification (iBAQ) intensity. The information of the relative abundance of each protein across different conditions was given by LFQ intensity. The mass proteome fraction (absolute abundance) of individual proteins was obtained using the iBAQ intensity of each protein to multiply the molecular weight (we referred to as "iBAQ mass" in table S3) and further normalized by the sum of the whole proteome (as iBAQ is a proxy of the copy number of each protein). The iBAQ mass of individual proteins together with the gene locus-tag were submitted to proteomaps website to obtain the Kyoto Encyclopedia of Genes and Genomes (KEGG) resource allocation map of *B. subtilis* cells (*32*).

Statistical analysis

The SDs (error bars) of data were analyzed with GraphPad Prism 8.0. Replicate numbers are specified in the captions of the figures where they appear. Data points for each biological replicates are displayed in the related figures.

Supplementary Materials

This PDF file includes:

Table S1

Legends for tables S2 to S4

Figs. S1 to S14

Other Supplementary Material for this manuscript includes the following:
Tables S2 to S4

REFERENCES AND NOTES

1. M. Scott, T. Hwa, Shaping bacterial gene expression by physiological and proteome allocation constraints. *Nat. Rev. Microbiol.* **21**, 327–342 (2023).
2. X. Dai, M. Zhu, Coupling of ribosome synthesis and translational capacity with cell growth. *Trends Biochem. Sci.* **45**, 681–692 (2020).
3. D. Molenaar, R. van Berlo, D. de Ridder, B. Teusink, Shifts in growth strategies reflect tradeoffs in cellular economics. *Mol. Syst. Biol.* **5**, 323 (2009).
4. M. Basan, T. Honda, D. Christodoulou, M. Horl, Y. F. Chang, E. Leoncini, A. Mukherjee, H. Okano, B. R. Taylor, J. M. Silverman, C. Sanchez, J. R. Williamson, J. Paulsson, T. Hwa, U. Sauer, A universal trade-off between growth and lag in fluctuating environments. *Nature* **584**, 470–474 (2020).
5. X. P. Hu, H. Dourado, P. Schubert, M. J. Lercher, The protein translation machinery is expressed for maximal efficiency in *Escherichia coli*. *Nat. Commun.* **11**, 5260 (2020).
6. S. Kostinski, S. Reuveni, Ribosome composition maximizes cellular growth rates in *E. coli*. *Phys. Rev. Lett.* **125**, 028103 (2020).
7. J. Bjorkeroth, K. Campbell, C. Malina, R. Yu, F. Di Bartolomeo, J. Nielsen, Proteome reallocation from amino acid biosynthesis to ribosomes enables yeast to grow faster in rich media. *Proc. Natl. Acad. Sci. U.S.A.* **117**, 21804–21812 (2020).
8. M. Eames, T. Kortemme, Cost-benefit tradeoffs in engineered lac operons. *Science* **336**, 911–915 (2012).
9. G. I. Lang, A. W. Murray, D. Botstein, The cost of gene expression underlies a fitness tradeoff in yeast. *Proc. Natl. Acad. Sci. U.S.A.* **106**, 5755–5760 (2009).
10. C. F. Pope, T. D. McHugh, S. H. Gillespie, Methods to determine fitness in bacteria. *Methods Mol. Biol.* **642**, 113–121 (2010).
11. M. Scott, C. W. Gunderson, E. M. Mateescu, Z. Zhang, T. Hwa, Interdependence of cell growth and gene expression: Origins and consequences. *Science* **330**, 1099–1102 (2010).
12. C. You, H. Okano, S. Hui, Z. Zhang, M. Kim, C. W. Gunderson, Y. P. Wang, P. Lenz, D. Yan, T. Hwa, Coordination of bacterial proteome with metabolism by cyclic AMP signalling. *Nature* **500**, 301–306 (2013).
13. G. W. Li, D. Burkhardt, C. Gross, J. S. Weissman, Quantifying absolute protein synthesis rates reveals principles underlying allocation of cellular resources. *Cell* **157**, 624–635 (2014).
14. Z. Tomáš, Quantitative insights into the cyanobacterial cell economy. *eLife* **8**, e42508 (2019).
15. M. Zhu, X. Dai, Growth suppression by altered (p)ppGpp levels results from non-optimal resource allocation in *Escherichia coli*. *Nucleic Acids Res.* **47**, 4684–4693 (2019).
16. J. Xia, B. J. Sánchez, Y. Chen, K. Campbell, S. Kasvandik, J. Nielsen, Proteome allocations change linearly with the specific growth rate of *Saccharomyces cerevisiae* under glucose limitation. *Nat. Commun.* **13**, 2819 (2022).
17. C. Wu, R. Balakrishnan, N. Braniff, M. Mori, G. Manzanarez, Z. Zhang, T. Hwa, Cellular perception of growth rate and the mechanistic origin of bacterial growth law. *Proc. Natl. Acad. Sci. U.S.A.* **119**, e2201585119 (2022).
18. A. Battesti, N. Majdalani, S. Gottesman, The RpoS-mediated general stress response in *Escherichia coli*. *Annu. Rev. Microbiol.* **65**, 189–213 (2011).
19. A. Oslizlo, P. Stefanic, I. Dogsa, I. Mandic-Mulec, Private link between signal and response in *Bacillus subtilis* quorum sensing. *Proc. Natl. Acad. Sci. U.S.A.* **111**, 1586–1591 (2014).
20. E. Biselli, S. J. Schink, U. Gerland, Slower growth of *Escherichia coli* leads to longer survival in carbon starvation due to a decrease in the maintenance rate. *Mol. Syst. Biol.* **16**, e9478 (2020).
21. M. Mori, S. Schink, D. W. Erickson, U. Gerland, T. Hwa, Quantifying the benefit of a proteome reserve in fluctuating environments. *Nat. Commun.* **8**, 1225 (2017).
22. R. Balakrishnan, R. T. de Silva, T. Hwa, J. Cremer, Suboptimal resource allocation in changing environments constrains response and growth in bacteria. *Mol. Syst. Biol.* **17**, e10597 (2021).
23. M. Mori, Z. Zhang, A. Banaei-Esfahani, J. B. Lalanne, H. Okano, B. C. Collins, A. Schmidt, O. T. Schubert, D. S. Lee, G. W. Li, R. Aebersold, T. Hwa, C. Ludwig, From coarse to fine: The absolute *Escherichia coli* proteome under diverse growth conditions. *Mol. Syst. Biol.* **17**, e9536 (2021).
24. T. Garland Jr., Trade-offs. *Curr. Biol.* **24**, R60–R61 (2014).
25. M. Kalamara, M. Spacapan, I. Mandic-Mulec, N. R. Stanley-Wall, Social behaviours by *Bacillus subtilis*: Quorum sensing, kin discrimination and beyond. *Mol. Microbiol.* **110**, 863–878 (2018).
26. D. Higgins, J. Dworkin, Recent progress in *Bacillus subtilis* sporulation. *FEMS Microbiol. Rev.* **36**, 131–148 (2012).
27. Y. Qin, L. L. Angelini, Y. Chai, *Bacillus subtilis* cell differentiation, biofilm formation and environmental prevalence. *Microorganisms* **10**, 1108 (2022).
28. M. J. Wiser, R. E. Lenski, A comparison of methods to measure fitness in *Escherichia coli*. *PLOS ONE* **10**, e0126210 (2015).
29. J. N. Barber, A. L. Sezmis, L. C. Woods, T. D. Anderson, J. M. Voss, M. J. McDonald, The evolution of coexistence from competition in experimental co-cultures of *Escherichia coli* and *Saccharomyces cerevisiae*. *ISME J.* **15**, 746–761 (2021).
30. J. E. González-Pastor, Cannibalism: A social behavior in sporulating *Bacillus subtilis*. *FEMS Microbiol. Rev.* **35**, 415–424 (2011).
31. J. E. González-Pastor, E. C. Hobbs, R. Losick, Cannibalism by sporulating bacteria. *Science* **301**, 510–513 (2003).
32. W. Liebermeister, E. Noor, A. Flamholz, D. Davidi, J. Bernhardt, R. Milo, Visual account of protein investment in cellular functions. *Proc. Natl. Acad. Sci. U.S.A.* **111**, 8488–8493 (2014).
33. F. Hu, Y. Liu, S. Li, Rational strain improvement for surfactin production: Enhancing the yield and generating novel structures. *Microb. Cell Fact.* **18**, 42 (2019).
34. T. Stein, *Bacillus subtilis* antibiotics: Structures, syntheses and specific functions. *Mol. Microbiol.* **56**, 845–857 (2005).
35. F. B. Rahman, B. Sarkar, R. Moni, M. S. Rahman, Molecular genetics of surfactin and its effects on different sub-populations of *Bacillus subtilis*. *Biotechnol. Rep. (Amst.)* **32**, e00686 (2021).
36. T. Tian, B. Sun, H. Shi, T. Gao, Y. He, Y. Li, Y. Liu, X. Li, L. Zhang, S. Li, Q. Wang, Y. Chai, Sucrose triggers a novel signaling cascade promoting *Bacillus subtilis* rhizosphere colonization. *ISME J.* **15**, 2723–2737 (2021).
37. N. M. Belliveau, G. Chure, C. L. Hueschen, H. G. Garcia, J. Kondev, D. S. Fisher, J. A. Theriot, R. Phillips, Fundamental limits on the rate of bacterial growth and their influence on proteomic composition. *Cell Systems* **12**, 924–944.e2 (2021).
38. M. Scott, S. Klumpp, E. M. Mateescu, T. Hwa, Emergence of robust growth laws from optimal regulation of ribosome synthesis. *Mol. Syst. Biol.* **10**, 747 (2014).
39. X. Dai, M. Zhu, M. Warren, R. Balakrishnan, V. Patsalo, H. Okano, J. R. Williamson, K. Fredrick, Y. P. Wang, T. Hwa, Reduction of translating ribosomes enables *Escherichia coli* to maintain elongation rates during slow growth. *Nat. Microbiol.* **2**, 16231 (2017).
40. M. Scott, T. Hwa, Bacterial growth laws and their applications. *Curr. Opin. Biotechnol.* **22**, 559–565 (2011).
41. H. H. Lee, N. Ostrov, B. G. Wong, M. A. Gold, A. S. Khalil, G. M. Church, Functional genomics of the rapidly replicating bacterium *Vibrio natriegens* by CRISPRi. *Nat. Microbiol.* **4**, 1105–1113 (2019).
42. S. A. Blackman, T. J. Smith, S. J. Foster, The role of autolysins during vegetative growth of *Bacillus subtilis* 168. *Microbiology* **144**, 73–82 (1998).
43. T. J. Smith, S. A. Blackman, S. J. Foster, Autolysins of *Bacillus subtilis:* Multiple enzymes with multiple functions. *Microbiology* **146**, 249–262 (2000).
44. H. Yamamoto, S. Kurosawa, J. Sekiguchi, Localization of the vegetative cell wall hydrolases LytC, LytE, and LytF on the *Bacillus subtilis* cell surface and stability of these enzymes to cell wall-bound or extracellular proteases. *J. Bacteriol.* **185**, 6666–6677 (2003).
45. R. Chen, S. B. Guttenplan, K. M. Blair, D. B. Kearns, Role of the sigmaD-dependent autolysins in *Bacillus subtilis* population heterogeneity. *J. Bacteriol.* **191**, 5775–5784 (2009).
46. S. J. Schink, E. Biselli, C. Ammar, U. Gerland, Death rate of *E. coli* during starvation is set by maintenance cost and biomass recycling. *Cell Syst.* **9**, 64–73.e3 (2019).
47. F. J. Slack, J. P. Mueller, M. A. Strauch, C. Mathiopoulos, A. L. Sonenshein, Transcriptional regulation of a *Bacillus subtilis* dipeptide transport operon. *Mol. Microbiol.* **5**, 1915–1925 (1991).
48. A. Koide, J. A. Hoch, Identification of a second oligopeptide transport system in *Bacillus subtilis* and determination of its role in sporulation. *Mol. Microbiol.* **13**, 417–426 (1994).
49. A. Zaprasis, J. Brill, M. Thüring, G. Wünsche, M. Heun, H. Barzantny, T. Hoffmann, E. Bremer, Osmoprotection of *Bacillus subtilis* through import and proteolysis of proline-containing peptides. *Appl. Environ. Microbiol.* **79**, 576–587 (2013).
50. S. Klumpp, M. Scott, S. Pedersen, T. Hwa, Molecular crowding limits translation and cell growth. *Proc. Natl. Acad. Sci. U.S.A.* **110**, 16754–16759 (2013).
51. M. Zhu, X. Dai, Stringent response ensures the timely adaptation of bacterial growth to nutrient downshift. *Nat. Commun.* **14**, 467 (2023).
52. B. Ni, R. Colin, H. Link, R. G. Endres, V. Sourjik, Growth-rate dependent resource investment in bacterial motile behavior quantitatively follows potential benefit of chemotaxis. *Proc. Natl. Acad. Sci. U.S.A.* **117**, 595–601 (2020).
53. D. Reznick, K. King, Antibiotic resistance: Evolution without trade-offs. *Nat. Ecol. Evol.* **1**, 66 (2017).
54. C. Michaux, S. Ronneau, R. T. Giorgio, S. Helaine, Antibiotic tolerance and persistence have distinct fitness trade-offs. *PLOS Pathog.* **18**, e1010963 (2022).

55. A. F. Bennett, R. E. Lenski, An experimental test of evolutionary trade-offs during temperature adaptation. *Proc. Natl. Acad. Sci. U.S.A.* **104**, 8649–8654 (2007).
56. V. Molle, M. Fujita, S. T. Jensen, P. Eichenberger, J. E. Gonzalez-Pastor, J. S. Liu, R. Losick, The Spo0A regulon of *Bacillus subtilis*. *Mol. Microbiol.* **50**, 1683–1701 (2003).
57. B. R. Belitsky, A. L. Sonenshein, Genetic and biochemical analysis of CodY-binding sites in *Bacillus subtilis*. *J. Bacteriol.* **190**, 1224–1236 (2008).
58. S. Schink, C. Ammar, Y. F. Chang, R. Zimmer, M. Basan, Analysis of proteome adaptation reveals a key role of the bacterial envelope in starvation survival. *Mol. Syst. Biol.* **18**, e11160 (2022).
59. F. Farahpour, M. Saeedghalati, V. S. Brauer, D. Hoffmann, Trade-off shapes diversity in eco-evolutionary dynamics. *eLife* **7**, e36273 (2018).
60. T. Ferenci, Trade-off mechanisms shaping the diversity of bacteria. *Trends Microbiol.* **24**, 209–223 (2016).
61. J. L. Weissman, S. Hou, J. A. Fuhrman, Estimating maximal microbial growth rates from cultures, metagenomes, and single cells via codon usage patterns. *Proc. Natl. Acad. Sci. U.S.A.* **118**, e2016810118 (2021).
62. G. M. Cook, M. Berney, S. Gebhard, M. Heinemann, M. Niederweis, Physiology of mycobacteria. *Adv. Microb. Physiol.* **55**, 81–182 (2009).
63. B. J. Campbell, D. L. Kirchman, Bacterial diversity, community structure and potential growth rates along an estuarine salinity gradient. *ISME J.* **7**, 210–220 (2013).
64. J. Li, R. L. Mau, P. Dijkstra, B. J. Koch, E. Schwartz, X. A. Liu, E. M. Morrissey, S. J. Blazewicz, J. Pett-Ridge, B. W. Stone, M. Hayer, B. A. Hungate, Predictive genomic traits for bacterial growth in culture versus actual growth in soil. *ISME J.* **13**, 2162–2172 (2019).
65. R. Mikkola, C. G. Kurland, Selection of laboratory wild-type phenotype from natural isolates of *Escherichia coli* in chemostats. *Mol. Biol. Evol.* **9**, 394–402 (1992).
66. B. B. Jorgensen, A. Boetius, Feast and famine--microbial life in the deep-sea bed. *Nat. Rev. Microbiol.* **5**, 770–781 (2007).
67. C. Liao, A. E. Blanchard, T. Lu, An integrative circuit-host modelling framework for predicting synthetic gene network behaviours. *Nat. Microbiol.* **2**, 1658–1666 (2017).
68. A. J. Lopatkin, J. J. Collins, Predictive biology: Modelling, understanding and harnessing microbial complexity. *Nat. Rev. Microbiol.* **18**, 507–520 (2020).
69. S. E. Finkel, Long-term survival during stationary phase: Evolution and the GASP phenotype. *Nat. Rev. Microbiol.* **4**, 113–120 (2006).
70. J. W. Payne, M. W. Smith, Peptide transport by micro-organisms. *Adv. Microb. Physiol.* **36**, 1–80 (1994).
71. P. Garai, K. Chandra, D. Chakravortty, Bacterial peptide transporters: Messengers of nutrition to virulence. *Virulence* **8**, 297–309 (2017).
72. P. R. Burkholder, N. H. Giles, Induced biochemical mutations in *Bacillus subtilis*. *Am. J. Bot.* **34**, 345–348 (1947).
73. A. M. Guérout-Fleury, N. Frandsen, P. Stragier, Plasmids for ectopic integration in *Bacillus subtilis*. *Gene* **180**, 57–61 (1996).
74. B. Härtl, W. Wehrl, T. Wiegert, G. Homuth, W. Schumann, Development of a new integration site within the *Bacillus subtilis* chromosome and construction of compatible expression cassettes. *J. Bacteriol.* **183**, 2696–2699 (2001).
75. T. T. P. Phan, L. T. Tran, W. Schumann, H. D. Nguyen, Development of P*grac*100-based expression vectors allowing high protein production levels in *Bacillus subtilis* and relatively low basal expression in *Escherichia coli*. *Microb. Cell Fact.* **14**, 72 (2015).
76. M. Zhu, H. Mu, F. Han, Q. Wang, X. Dai, Quantitative analysis of asynchronous transcription-translation and transcription processivity in *Bacillus subtilis* under various growth conditions. *iScience* **24**, 103333 (2021).
77. M. Basan, M. Zhu, X. Dai, M. Warren, D. Sevin, Y. P. Wang, T. Hwa, Inflating bacterial cells by increased protein synthesis. *Mol. Syst. Biol.* **11**, 836 (2015).
78. Z. Chen, P. Srivastava, B. Zarazúa-Osorio, A. Marathe, M. Fujita, O. A. Igoshin, *Bacillus subtilis* histidine kinase KinC activates biofilm formation by controlling heterogeneity of single-cell responses. *MBio* **13**, e0169421 (2022).
79. F. Meier, A. D. Brunner, S. Koch, H. Koch, M. Lubeck, M. Krause, N. Goedecke, J. Decker, T. Kosinski, M. A. Park, Online parallel accumulation–serial fragmentation (PASEF) with a novel trapped ion mobility mass spectrometer. *Mol. Cell. Proteomics* **17**, 2534–2545 (2018).
80. S. Tyanova, T. Temu, J. Cox, The MaxQuant computational platform for mass spectrometry-based shotgun proteomics. *Nat. Protoc.* **11**, 2301–2319 (2016).

Acknowledgments: We thank members of the Terry Hwa laboratory (UCSD) for useful discussions during various stages of the work. We thank J. Zhang (Shanghai Jiao Tong University), Z. Zhou (Jiangnan University), and M. Sun (Huazhong Agricultural University) for providing the pHT01 vector, the pAX01 vector, and the pDG1730 vector, respectively. **Funding:** This study was supported by the National Natural Science Foundation of China, grants 32022001 and 32270034 (M.Z.); the National Natural Science Foundation of China, grant 31970027 (X.D.); the Changjiang Young Scholar Program of Chinese Ministry of Education (X.D.); the National Key Research and Development Program of China, grant 2022YFF1000400 (X.D. and M.Z.); the Natural Science Funds for Distinguished Young Scholar of Hubei Province, 2022CFA044 (M.Z.); and the Fundamental Research Funds for the Central Universities (M.Z. and X.D.). **Author contributions:** Conceptualization: X.D. and M.Z. Methodology: M.Z. and X.D. Investigation: M.Z., Q.W., H.M., F.H., Y.W., and X.D. Supervision: X.D. Writing—original draft: X.D. and M.Z. Writing—review and editing: X.D. and M.Z. **Competing interests:** The authors declare that they have no competing interests. **Data and materials availability:** All data needed to evaluate the conclusions in the paper are present in the paper and/or the Supplementary Materials. The mass spectrometry proteomics data have been deposited to the ProteomeXchange Consortium via the PRIDE partner repository with the dataset identifier PXD039192.

Submitted 2 February 2023
Accepted 25 August 2023
Published 27 September 2023
10.1126/sciadv.adg9733